6-15-2018

Seismic Imaging of the Main Frontal Thrust in Nepal Reveals a Shallow Décollement and Blind Thrusting

Rafael V. Almeida
Nanyang Technological University

Judith Hubbard
Nanyang Technological University

Lee Liberty
Boise State University

Anna Foster
Nanyang Technological University

Soma Nath Sapkota
Department of Mines and Geology

Publication Information

Almeida, Rafael V.; Hubbard, Judith; Liberty, Lee; Foster, Anna; and Sapkota, Soma Nath. (2018). "Seismic Imaging of the Main Frontal Thrust in Nepal Reveals a Shallow Décollement and Blind Thrusting". *Earth and Planetary Science Letters, 494,* 216-225. https://doi.org/10.1016/j.epsl.2018.04.045

Earth and Planetary Science Letters 494 (2018) 216–225

Contents lists available at ScienceDirect

Earth and Planetary Science Letters

www.elsevier.com/locate/epsl

Seismic imaging of the Main Frontal Thrust in Nepal reveals a shallow décollement and blind thrusting

Rafael V. Almeida [a,*], Judith Hubbard [a,b], Lee Liberty [c], Anna Foster [a,d], Soma Nath Sapkota [e]

[a] Earth Observatory of Singapore, Nanyang Technological University, Singapore
[b] Asian School of the Environment, Nanyang Technological University, Singapore
[c] Department of Geosciences, Boise State University, ID, USA
[d] Département des sciences de la Terre et de l'atmosphère, Université du Québec à Montréal, Canada
[e] Department of Mines and Geology, Kathmandu 44600, Nepal

ARTICLE INFO

Article history:
Received 29 September 2017
Received in revised form 19 April 2018
Accepted 20 April 2018
Available online xxxx
Editor: R. Bendick

Keywords:
Main Frontal Thrust
Himalayan earthquakes
reflection seismic
paleoseismology
tectonic geomorphology

ABSTRACT

Because great earthquakes in the Himalaya have an average recurrence interval exceeding 500 yr, most of what we know about past earthquakes comes from paleoseismology and tectonic geomorphology studies of the youngest fault system there, the Main Frontal Thrust (MFT). However, these data are sparse relative to fault segmentation and length, and interpretations are often hard to validate in the absence of information about fault geometry. Here, we image the upper two km of strata in the vicinity of the fault tip of the MFT in central Nepal (around the town of Bardibas) applying a pre-stack migration approach to two new seismic reflection profiles that we interpret using quantitative fault-bend folding theory. Our results provide direct evidence that a shallow décollement produces both emergent (Patu thrust) and blind (Bardibas thrust) fault strands. We show that the décollement lies about 2 km below the land surface near the fault tip, and steps down to a regional 5 km deep décollement level to the north. This implies that there is significant variation in the depth of the décollement. We demonstrate that some active faults do not reach the surface, and therefore paleoseismic trenching alone cannot characterize the earthquake history at these locations. Although blind, these faults have associated growth strata that allow us to infer their most recent displacement history. We present the first direct evidence of fault dip on two fault strands of the MFT at depth that can allow terrace uplift measurements to be more accurately converted to fault slip. We identify a beveled erosional surface buried beneath Quaternary sediments, indicating that strath surface formation is modulated by both climate-related base level changes and tectonics. Together, these results indicate that subsurface imaging, in conjunction with traditional paleoseismological tools, can best characterize the history of fault slip in the Himalaya and other similar thrust fault systems.

1. Introduction: great earthquakes in the Himalaya

The Himalaya (Fig. 1) represents one of the few regions on Earth where great, surface-rupturing thrust earthquakes occur on land. This, combined with the vulnerability of the densely populated Gangetic Plain south of the Himalaya, produces high seismic risk in this region (Bilham, 2014). The Main Frontal Thrust (MFT) in Nepal is the youngest and southernmost structure in the Himalayan Fold and Thrust belt (Fig. 1; Gansser, 1964). This thrust roots into a regional décollement, or bed-parallel fault, known as the Main Himalayan Thrust (MHT) that underlies the entire Himalaya and represents the contact between the Indian and Asian plates (Fig. 1A; Seeber and Armbruster, 1981; Zhao et al., 1993).

Since the identification of the MFT and MHT, questions have been raised about how this fault system slips in earthquakes, and whether this slip is surface emergent. Seeber and Armbruster (1981) proposed that the MHT extends past the MFT underneath the Gangetic Plain, and that coseismic slip during great earthquakes remains blind. Schelling and Arita (1991) and Delcaillau (1992) were among the first to depict the MFT as the frontal ramp of the MHT, raising the possibility that coseismic slip could reach the surface. Wesnousky et al. (1999) and Lave and Avouac (2000) studied uplifted river terraces and concluded that the Holocene convergence rate on the MFT is similar to the geodetically deter-

* Corresponding author.
E-mail address: ralmeida@ntu.edu.sg (R.V. Almeida).

https://doi.org/10.1016/j.epsl.2018.04.045

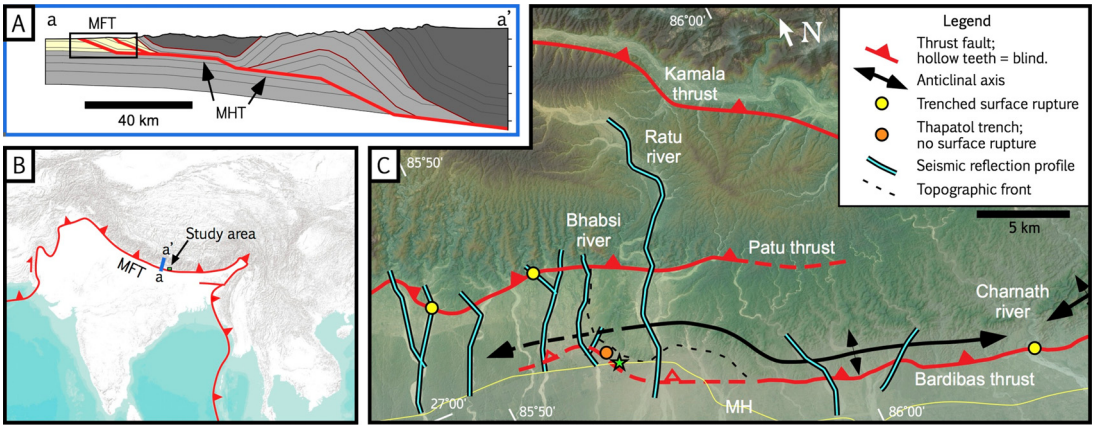

Fig. 1. (A) General cross-section a–a′ across the Himalaya, after Hubbard et al. (2016). Bold red line indicates active faults and thin red lines represent inactive faults; MFT, Main Frontal Thrust; MHT, Main Himalayan Thrust. (B) Location map, showing the kinematic boundary between the Indian and Asian plates (red line with teeth), cross-section a–a′ (blue line), and study area. (C) Study area, showing locations of seismic profiles. Star represents town of Bardibas. MH, Mahendra Highway. Basemaps for (B) and (C) from ESRI, USGS, NOAA SRTM data (Jarvis et al., 2008).

mined convergence rate between India and southern Tibet. This implies that elastic strain is released during great earthquakes on the MFT. Over the past 20 years, trenching studies have reported surface ruptures in the Himalaya, finding evidence of the 1255 (e.g. Nakata et al., 1998; Lave et al., 2005; Wesnousky et al., 2017) and 1934 (Sapkota et al., 2013; Bollinger et al., 2014) earthquakes in Nepal, as well as other ruptures (e.g. Kumar et al., 2006). This has led to a new paradigm: that great earthquakes in the Himalaya commonly breach the surface along the trace of the MFT.

2. Local structure and stratigraphy

Our study area is located in the Himalayan foreland fold and thrust belt, around the town of Bardibas in central Nepal (Fig. 1). The study region encompasses a right-step of the Himalayan range front, with two overlapping northwest–southeast trending fault strands: the northern Patu thrust, and the southern Bardibas thrust. Analyses of trenches and river cuts across the Patu thrust demonstrate that it ruptured in both 1255 and 1934 (Sapkota et al., 2013; Bollinger et al., 2014). However, a trench of the Bardibas thrust near the town of Bardibas did not find a surface rupture, but rather a fold scarp (Fig. 1; Bollinger et al., 2014). The faults in this area deform the Siwalik Group, a ∼5 km thick package of mid-Miocene to Pliocene fluvial strata with 2–20 m alternating siltstone and sandstone layers (Delcaillau, 1992). This stratigraphic group is generally divided into Lower, Middle and Upper Siwalik (Gansser, 1964; Delcaillau, 1992). The Lower Siwalik consists of alternating gray fine sandstones and siltstones. The beds attain thicknesses of a few meters and are strongly lithified. The Middle Siwalik consists of massive tan sandstone layers (up to 10s of m in thickness) which occasionally have a characteristic “salt and pepper” texture caused by mica grains. There are occasional lenses of conglomerates. The Upper Siwalik consists of conglomeratic channel deposits and boulder beds. The contact between the latter two units is often transitional, as the proportion of sand to gravel beds changes. However, the Middle to Upper Siwalik transition spans ∼100 m on the Ratu River. Further description of the stratigraphy of this area can be found in Delcaillau (1992) and Dhital (2015).

3. Seismic data from central Nepal

We used a vibroseis source to acquire ten high resolution seismic profiles across the MFT during 2014 and 2015 (Fig. 1). The seismic lines follow seasonal riverbeds that are generally orthogonal to the range front. The resulting pre-stack depth migrated seismic reflection profiles image to ∼2 km below the surface and provide a robust interval seismic velocity estimate for the upper 500 m. Here, we present two profiles: one along the Ratu River that cuts across both the Patu and Bardibas thrusts, and one along the Bhabsi River to the west of Bardibas (Fig. 1). In the following sections, we discuss the fault location and orientation, faulting style, growth strata and axial surfaces associated with the deformation for each thrust, and estimate the amount of shortening. We highlight our findings that have implications for regional tectonic studies, and then discuss our results in the context of seismic hazard studies. Information on data acquisition and processing can be found in the supplementary materials.

4. Interpretation of seismic data

We use the seismic reflection lines for the Ratu River and Bhabsi River to study the geometry of the fault systems, the amount of shortening that has occurred on these faults, and to infer the development of the shallow stratigraphy. For the structural aspect of this study, we combine the data with surface observations and use classic methods of seismic interpretation, as well as fault-bend fold, shear fault-bend fold, or fault-propagation fold theory as appropriate for each locality.

4.1. The Patu thrust and related deformation, Ratu River profile

Along the Ratu River profile (Fig. 2), the north-dipping Patu thrust is exposed on the river banks at common-depth point (CDP) ∼4000. Folded strata, observed both in seismic and at the surface, form a small anticline approximately 0.25 km north of the main thrust (CDP ∼3900), and then a larger anticline 1.5 km to the north (CDP ∼3300). The region directly below the crest of the larger anticline is not imaged due to a sharp bend in the river that restricted source points in that area. Otherwise, the Ratu River profile reflections are well defined, showing dip magnitudes and directions consistent with surface measurements, and occasional fault-plane reflections.

In particular, the well imaged northern axial surface of the anticline at CDP ∼2400 (northernmost dashed green line in Fig. 2), separates flat-lying beds to the north from north-dipping beds to the south. This abrupt transition in reflector or bed dip is also observed in outcrop. Across the axial surface, continuous reflectors can be traced through the fold to a depth of ∼1500 m below sea level (bsl; ∼2000 m below land surface). We observe that the axial surface bisects the fold, and infer that the folding is accommodated by flexural slip (i.e., slip along bedding planes) as the hanging wall rocks slide through the axial surface and up the fault ramp. We

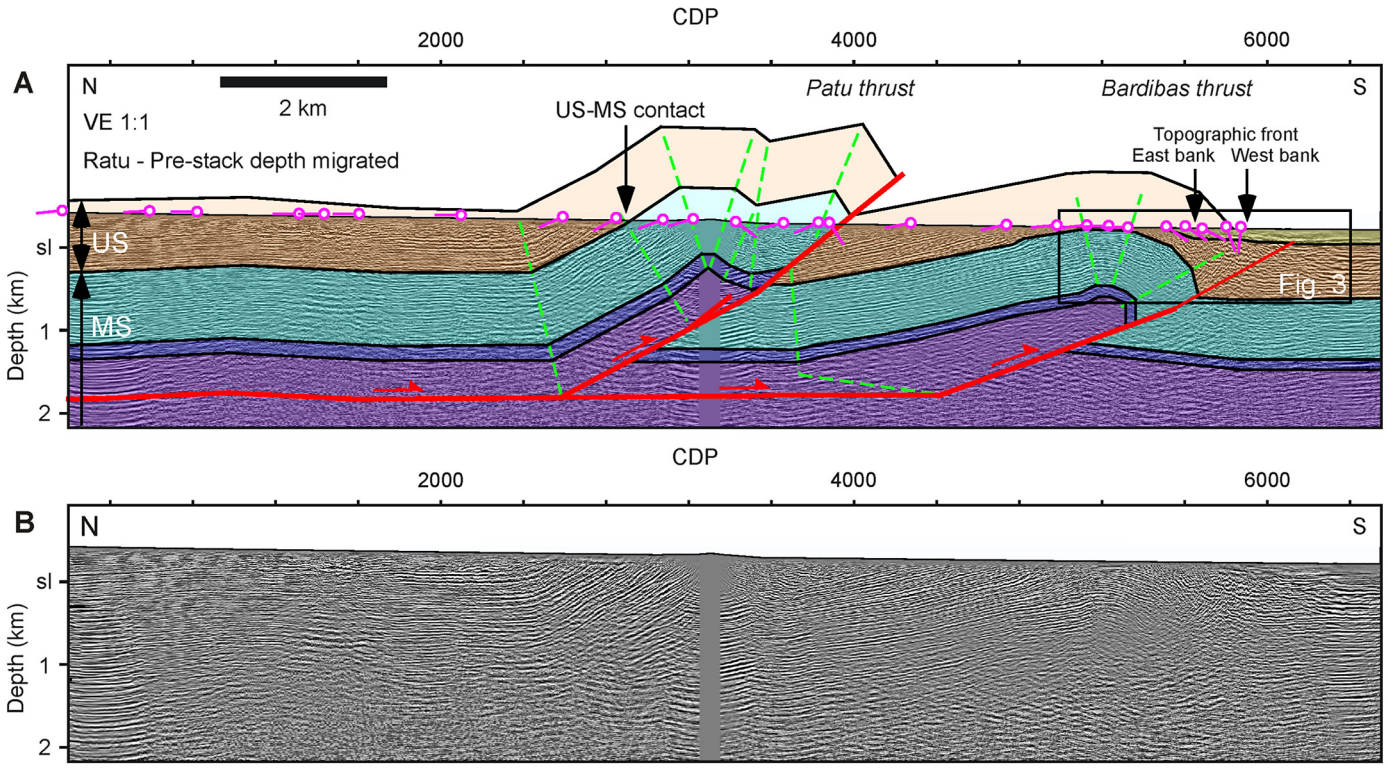

Fig. 2. (A) Ratu River seismic profile (post-stack depth-migrated, no vertical exaggeration), with interpretation (thrusts, red; axial surfaces, green); mean topography (thin black line above seismic data) and projected dips (magenta tick marks) are detailed in Fig. S1; colored shading to aid in visualizing continuous layers. Topographic front geometry shown in Fig. 1C. Contact between Upper Siwaliks (US, light orange layer) and Middle Siwaliks (MS, cyan layer) observed in the field. Dark blue and purple layers do not represent specific stratigraphic units, but rather are placed there to highlight shape of deformed strata. Black box shows location of Fig. 3. (B) Uninterpreted image (larger version in Fig. S3). CDP spacing is 2.5 m. Depth measurements are with respect to sea level (sl).

therefore interpret this feature as a fault-bend fold (Suppe, 1983; Shaw et al., 2005). However, the presence of anticlines near the fault tip indicates that there was likely a previous stage of fault-propagation folding (Jamison, 1987). Thus, in the early stage of deformation, the fault propagated towards the land surface as it slipped, and has since broken through, as demonstrated by its exposure at the surface.

To interpret the subsurface geometry of the Patu thrust, we start with the fault's surface exposure at CDP 3900. We map the fault at depth following a 39° north-dipping reflection that extends directly to the surface fault exposure. This fault plane reflection cuts a well imaged zone of more gently dipping reflectors. Where the fault plane reflection is not imaged (between 0 and ~60 m bsl), we extend our interpretation of the fault at the same dip as the hanging wall beds (28° north), consistent with fault-bend folding theory. Since the décollement is a bedding parallel fault, it is not possible to distinguish fault plane reflections from bedding plane reflections, and we must instead rely on geometrical relations between the fault ramp and the axial plane to determine its depth. The axial surface is well defined as the change from more or less horizontal beds, to north dipping beds (the location in the seismic line matches the observed location in the field). The fault is defined as the contact between the north dipping beds in the hanging wall of the Patu thrust and the horizontal beds in the footwall of the fault (Fig. 2). We extend the fault down to its intersection with the axial surface, thus defining the depth of the décollement (~1.8 km bsl, or 2.2 km below the surface).

4.2. The Bardibas thrust and related deformation, Ratu River profile

To the south of the Patu thrust, slip on the Bardibas thrust has formed a ~4 km wide asymmetric anticline (Fig. 2). Near the crest of the anticline at CDP 5300, the seismic image shows beds rolling over into the front limb. North-dipping reflections associated with the anticline's back limb matches mapped surface dips, and these reflections terminate to the north, overridden by the Patu thrust. This 10–12° dipping back limb is much broader than the front limb and dips more gently than the back limb of the Patu thrust anticline. The strata of the Bardibas front limb are imaged up to a dip of ~45° near CDP 5600 (Fig. 3). South of these steep dips, we note a ~500–1000 m wide poorly imaged region that is likely the result of beds steepening to beyond 45°. This interpretation is consistent with surface measurements of bedding attitudes that reach vertical and are even locally overturned at the southernmost part of the anticline forelimb (Figs. S1, S5C). An asymmetric fold typically forms in the hanging wall of a thrust fault that is propagating towards the surface (Jamison, 1987). Thus, we interpret that this zone of poor imaging as in the hanging wall of the fault. In addition, there appears to be minor deformation (possibly an incipient fault) that is caused by tightening of the overall anticline, visible between CDP 5200 at a depth of ~600 m below sea level and CDP 4800 at a depth of ~80 m below sea level (Fig. 2B).

The topographic front associated with the Bardibas thrust is oblique to the river, and therefore to our seismic line (Fig. 1). On the west bank of the Ratu River, the topographic front is located at CDP ~5900, while on the east bank it is at CDP ~5600. If there were a fault cropping out at the front, we would expect it to be well imaged as it would cut through the continuous reflections of the anticline crest and forelimb. However, our seismic data suggest that there is no surface expression of the fault. Instead, we identify a panel of ~30° north dipping reflections that lies ~600 m below the topographic front (400 m bsl). These subparallel reflections are likely an artifact of 3D effects caused by the local obliquity of the fault to our seismic profile. This produces out of plane reflections that can only be properly imaged using a 3D seismic imaging ap-

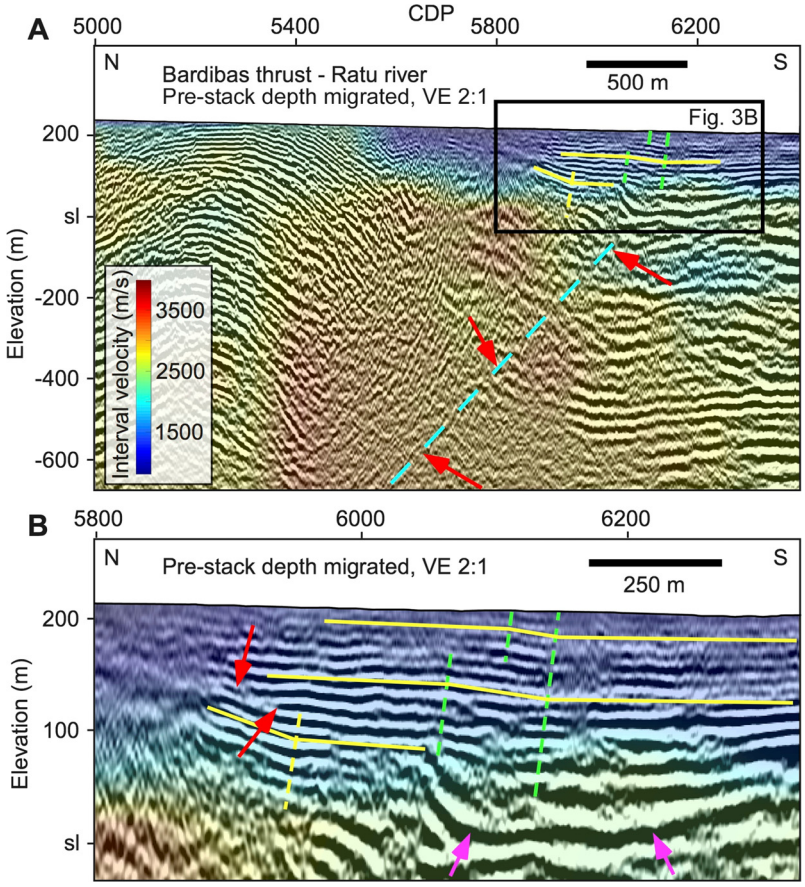

Fig. 3. (A) Close-up of the Bardibas thrust imaged along the Ratu River (location shown in Fig. 2), showing kink band in the fluvial sediments. Seismic image is post-stack depth-migrated and shown at 2:1 vertical exaggeration (VE) to emphasize gently dipping kink. Continuous reflections are emphasized with yellow lines. Green dashed lines represent the axial surfaces that bound the kink band. Yellow dashed line marks the axial surface for the folded panel. Red arrows indicate fault-plane reflections and fault plane is drawn as dashed blue line. Interval velocities are calculated by inverse ray tracing during pre-stack depth migration. (B) Further close-up of the kink band showing the abrupt decrease in its width. Red arrows point to onlap of fluvial strata onto folded panel. Magenta arrows show location of scour surface interpreted as an incised valley. CDP spacing is 2.5 m. Depth measurements are with respect to sea level (sl).

proach. We interpret that the location of the fault is marked by the termination of a packet of strong reflectors south of the inferred fault at ∼500 m bsl and CDP ∼5800 (Fig. 3; dashed blue line and red arrows in Fig. 3A). We map the upper part of the thrust (southernmost thin red line, Fig. 2) at the base of the poorly imaged zone that we interpret to represent steep dips.

In order to interpret the fault geometry, we extend the fault down-dip from the observed fault-plane reflection. Below 800 m bsl and north of ∼CDP 5500 our seismic data show that the Bardibas fault becomes less steep (20° dip) and separates gently north-dipping reflectors in the hanging wall from a zone of mottled seismic reflectors in the footwall (bold red line in Fig. 2). We extend the fault to the depth of the décollement identified for the Patu thrust. We note an axial surface close to the northern edge of the backlimb, below the Patu thrust at CDP ∼3700. As was the case for the Patu thrust, this axial surface bisects the bend between horizontal reflections and gently dipping reflections, consistent with fault-bend folding. However, the axial surface does not extend to the intersection between the Bardibas thrust and the décollement and we must allow a bend in the axial surface towards the bottom of the hanging wall strata in order for it to reach this intersection (kinked, dashed green line in Fig. 2). This axial surface geometry and wide, gently dipping back limb observed in the Bardibas thrust is characteristic of pure shear fault-bend folds, in which the stratigraphic interval spanned by the kinked axial surface represents the region that deforms with a component of pure shear (Suppe et al., 2004). Thus, we use a shear fault-bend fold model (Suppe et al., 2004) with fault propagation around the tip to interpret the geometry of the Bardibas thrust. Additionally, in a shear fault-bend fold, the fault dips more steeply than the beds in the back limb, consistent with the observed 20° dipping fault-plane reflection and 12° dipping beds. The Bardibas thrust is located below the continuous dipping reflections in the backlimb. If this structure were a non-shear fault-bend fold, the width of the back limb (∼4 km) would equal the amount of slip that has occurred on the fault. However, the offset layers in the seismic profile show significantly less slip, with slip decreasing towards the tip as is typical for a fault-propagation fold. Furthermore, at a depth of ∼500 m bsl there is a footwall syncline, likely related to the propagation towards the surface of the Bardibas thrust.

When we extend the Bardibas thrust fault plane reflector updip, it projects to the surface ∼1 km south of the topographic range front where the ground surface is flat and shallow reflections are continuous (highlighted in yellow in Fig. 3). However, in the shallow subsurface (upper 200 m) there is evidence for at least one kink band, which accommodates ∼15 m of uplift (CDP 6100; kink band bound by dashed green lines in Fig. 3). This kink band is divided in two parts. In the uppermost section the kink band is approximately half the width of the lower section. To the north, we observe that the layers that are folded by this kink band onlap a south-dipping panel of strata (north of yellow dashed line, Fig. 3) about 100 m below the surface (red arrows in Fig. 3B). This geometry implies that the onlapped south dipping panel has

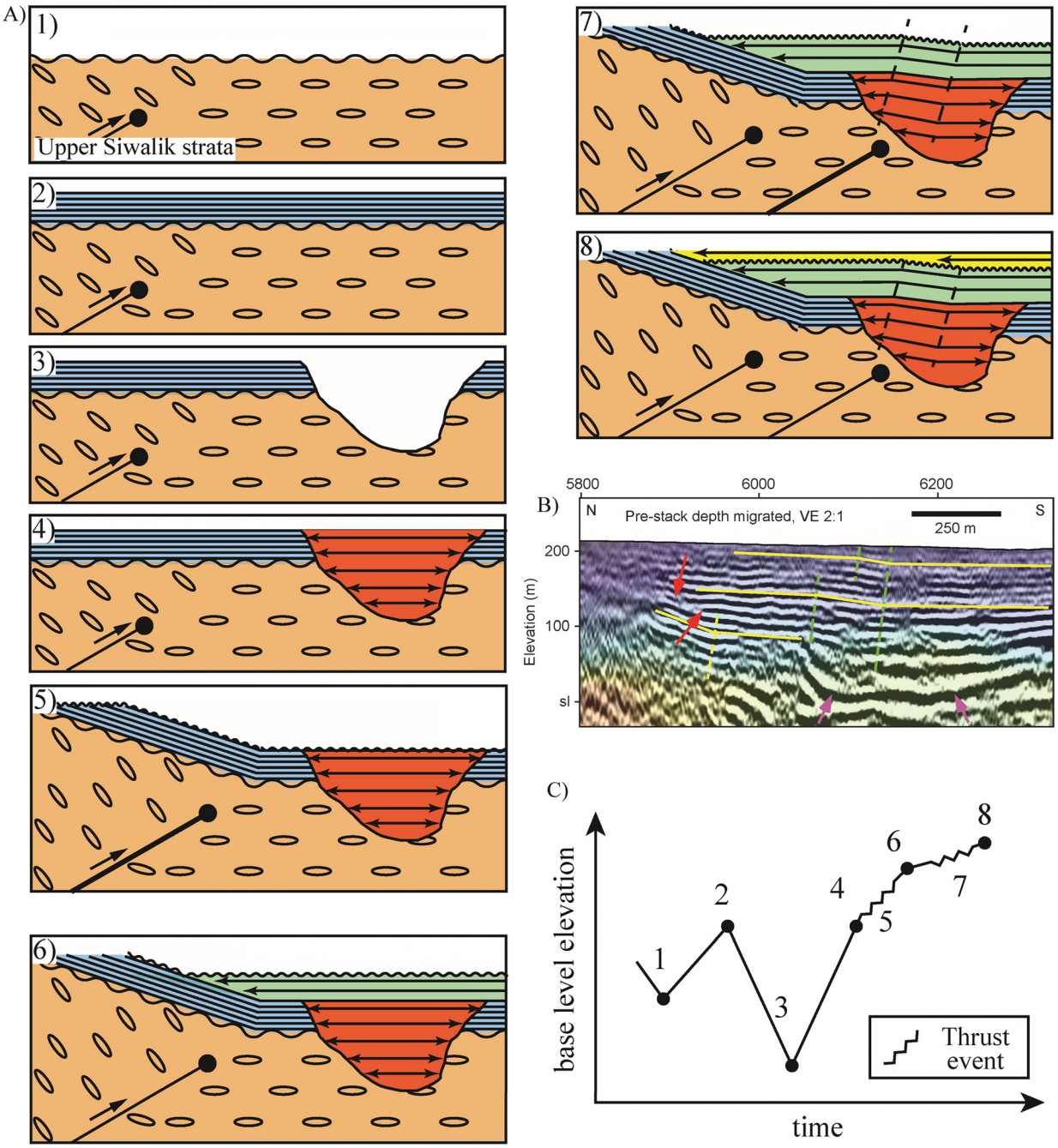

Fig. 4. Cartoon sections showing base level changes interpreted to have occurred in the footwall of the Bardibas thrust. The erosion and deposition of strata are inferred to be directly related to these changes. A) One possible step-by-step development of the shallow stratigraphy observed in the Ratu profile (Fig. 3B). 1) River bevels the top of the Bardibas anticline; 2) Blue strata are deposited due to base level rise; 3) Subsequent base level drop produces incised valley that cuts into Upper Siwalik strata; 4) Incised valley is filled by sediments; 5) Slip on the Bardibas thrust folds the blue strata (step 3 and 5 could have occurred interchangeably); 6) Green strata are deposited onlapping onto the folded blue strata; 7) Slip is transferred to a southern strand of the Bardibas thrust and creates a kink band ahead of the fault tip; 8) Yellow strata are deposited onlapping onto the kink band. This schematic does not show a final slip event on the southern strand of the Bardibas fault (i.e. another instance of step 7) that creates the small kink band shown in the shallowest part of the seismic data in part (B). Long axis of ovals in Upper Siwalik (brown) strata represent approximate dips of strata. Arrowheads represent onlapping stratal terminations. Blind fault tip shown as circle at end of fault. Panels where the fault is bold represent periods of thrusting. B) Seismic profile of frontal Ratu section from Fig. 3B for comparison. Red arrows point to onlap of fluvial strata onto folded panel. Magenta arrows show location of scour surface interpreted as an incised valley. CDP spacing is 2.5 m. Depth measurements are with respect to sea level (sl). C) Schematic plot of base level change over time. The numbered dots correspond to the panels in part (A). The time between these steps is unknown and the dots representing the relative base level elevation at each stage are equally spaced in time.

been inactive since the deposition of these sediments, and that the active deformation has migrated south by about 400 m. This deformation front migration may be related to either the propagation of the fault tip towards the south over time, or a splay of the fault in the north that was active prior to the current southern splay. The poor resolution in this part of the seismic profile does not allow us to distinguish between these scenarios. We present a possible sequence of events in Fig. 4. However, in either case, this geometry indicates that a component of deformation has reached the near-surface south of the topographic front, resulting in folding of the strata ahead of the tip of the fault, rather than faulting. Although the fluvial strata appear folded all the way to the surface, the small

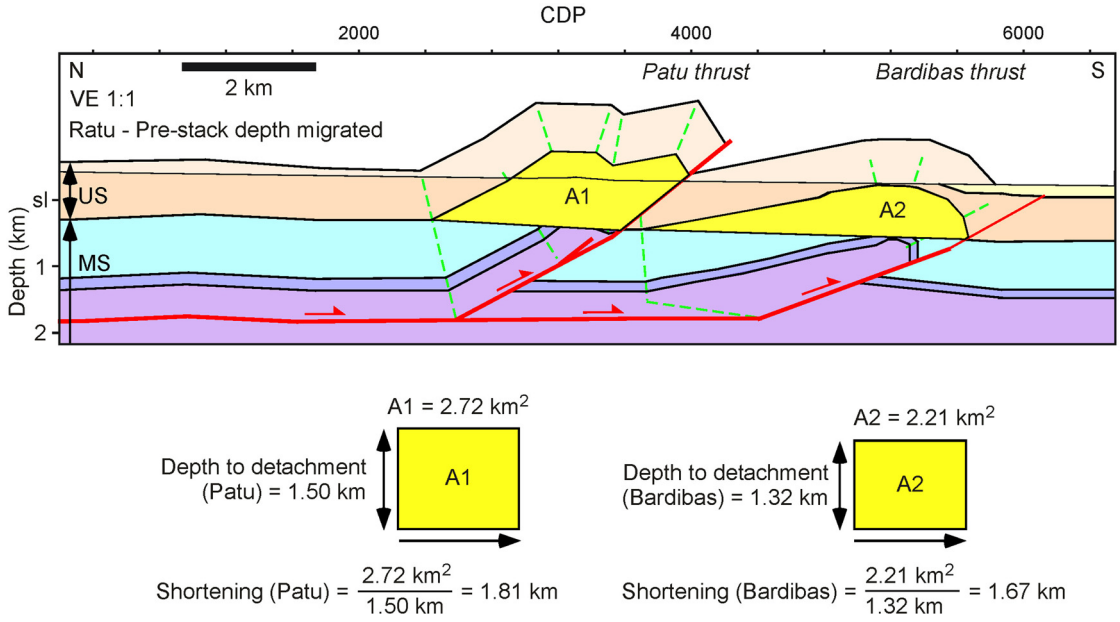

Fig. 5. Interpretation from Ratu River seismic profile (Fig. 2) illustrating the area-uplift methodology used to estimate the shortening accommodated on the Bardibas and Patu thrusts. Profile is not vertically exaggerated. CDP spacing is 2.5 m. Depth measurements are with respect to sea level (sl).

inferred uplift has no topographic expression because young fluvial sediments have been deposited above the uplift, eroding and/or burying the kink. We also note that between CDP 6100–6200, at a depth of ∼130 m below the surface, there is a clear scour surface (magenta arrows in Fig. 3B) that is consistent with an incised valley (Dalrymple et al., 1994) with a depth of ∼ 90 m, presumably related to base level fall of the regional fluvial system (Fig. 4). In summary, 1) there is no place where the Bardibas fault daylights and 2) to the south of the topographic front, shallow sediments are deformed. Thus, we describe the Bardibas thrust as a blind fault beneath the Ratu River.

4.3. Stratigraphy, Ratu River profile

We define the stratigraphy in the hanging wall of the Patu thrust by using the contact between the Upper and Middle Siwalik units (Fig. S5A, B), which crops out at CDP ∼2900 (Fig. 2). Based on our observations, the Middle Siwalik is exposed southward of that location until the surface trace of the Patu thrust. Based on the topography along strike of the seismic profile, we suggest that the top of the Upper Siwalik is ∼100 m above the river level north of the axial surface at CDP 2400; at this location, the cliffs on either side of the river rise ∼40 m–50 m. Based on this geometry, the Upper Siwalik at this location should be ∼650–850 m thick.

In order to extend our stratigraphic correlations across the profile, we assume that the depths of undeformed stratigraphic contacts are relatively constant. However, south of the Bardibas thrust, we note that there is a layer ∼175 m thick of unusually low prestack depth migrated interval seismic velocities (<2000 m/s, Fig. 3) that correlates with fine layering in the seismic reflection data. We interpret that this is a package of younger fluvial sediments deposited conformably above the Upper Siwalik due to fluvial aggradation (i.e. vertical buildup of a sedimentary sequence, Fig. S5D) related to relative base level changes. These sediments vary in thickness along the profile with a minimum thickness of ∼1.5 m in the core of the Bardibas thrust anticline, as exposed by a construction site along the river (Fig. S5D), and are deposited with an angular unconformity in the hanging wall of the Bardibas thrust. This forces the Siwalik contacts below this level to deeper levels than on the northern side of the profile. Based on this interpretation, we note that the Middle Siwaliks are just below the surface in the crest of the Bardibas thrust. This is consistent with our field observations that reveal rocks within the crest of the Bardibas thrust correspond to transitional strata between Upper and Middle Siwalik.

To accommodate this stratal geometry we allow the Siwalik strata to thin towards the south. This is consistent with the depositional setting of these strata within a foreland basin system, influenced by both regional subsidence and orogenic uplift (DeCelles and Giles, 1996). We also interpret a gentle depositional dip towards the south that is consistent with the fact that at least part of the Upper Siwalik is composed of alluvial fan or braided river materials deposited in the piedmont of the Himalayan wedge (Dhital, 2015). Based on the difference in elevation of the top of the Upper Siwalik in the north vs. south parts of the profile, and correcting for the amount of shortening across the two faults (Section 4.4), we calculate that the original depositional dip of the top of the Upper Siwalik was 1.6° to the south, which is larger than the dips of the modern large alluvial fans in front of the Himalaya (0.3°–0.6°; Dubille and Lave, 2015; Dingle et al., 2016), similar to the depositional dip of the smaller alluvial fans deposited in the modern piedmont (1.5° in the vicinity of the seismic lines) and smaller than the depositional dips measured on alluvial fans in arid environments (∼3°; Blair and McPherson, 2009).

4.4. Shortening estimates, Ratu River profile

In order to estimate shortening on the Patu and Bardibas thrusts, we use an area-of-uplift calculation (e.g. Lave and Avouac, 2000). We select an arbitrary stratigraphic horizon (in this case, the contact between the Upper and Middle Siwalik) and, from a location where the horizon is undeformed, measure the depth to the décollement; in this case, 1.50 km for the Patu thrust and 1.32 km for the Bardibas thrust. We then assume that area is conserved, i.e. that the area displaced during shortening is equal to the area now uplifted above its original level. We can estimate the amount of shortening by dividing this area by the depth to the décollement.

Fig. 5 shows the results of this calculation for both the Patu and Bardibas thrusts. We find that the Patu thrust has accommo-

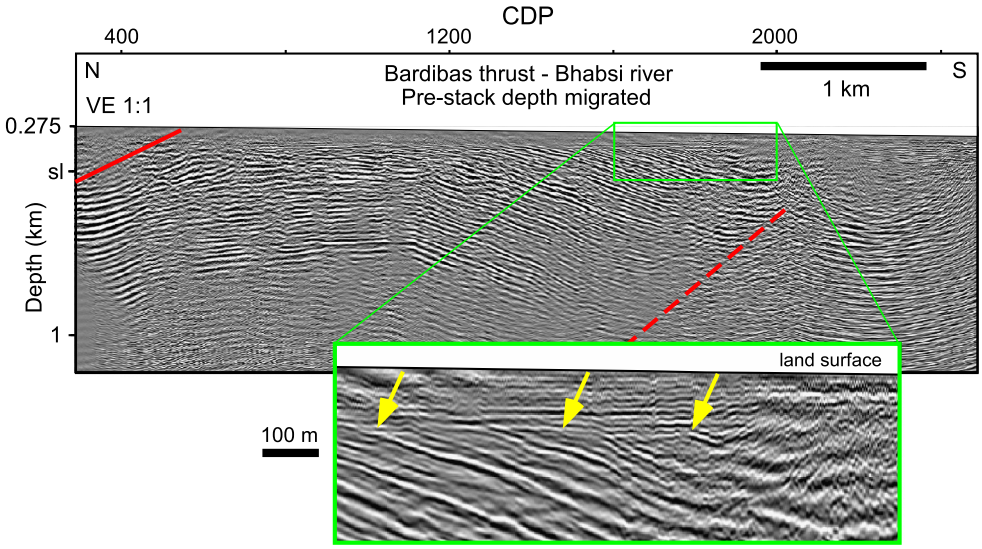

Fig. 6. Bhabsi River seismic profile (post-stack depth-migrated). Inset: Close-up of the buried angular unconformity from the Bhabsi River profile. Arrows show angular unconformity between tilted Siwalik strata and subhorizontal fluvial sediments. Approximate locations of the Patu and Bardibas thrusts, on the northern and southern end of the line respectively, are shown as dashed lines. CDP spacing is 2.5 m. Depth measurements are with respect to sea level (sl).

dated ~1.8 km of shortening, while the Bardibas thrust has accommodated ~1.7 km of shortening. We note that this calculation assumes that there is no movement of material into or out of the plane of this cross section and does not consider other shortening mechanisms such as compaction, and thus represents a minimum estimate.

4.5. Bhabsi river profile

The Bhabsi river profile is shorter than the Ratu profile and spans the distance between the Bardibas and Patu thrust. We could not acquire seismic data north of the Patu thrust here because the river becomes too sinuous. Beneath the Bhabsi River (Fig. 1), the Bardibas thrust has produced a symmetric anticline in the Siwalik strata that has been beveled and buried beneath 30–80 m of young fluvial sediments (Fig. 6). Because this is an anticline rather than simply north-dipping strata in the hanging wall of a fault, the structure must reflect some component of either detachment folding, fault-propagation folding, or both (Jamison, 1987; Mitra, 2002). The northern limb has dips between 4°–21° to the north and the southern limb dips 13°–27° to the south. The southern limb of the anticline terminates abruptly along a linear trend dipping 45° to the north into a poor imaging zone. It is unclear what has caused this poor imaging; perhaps a more steeply dipping panel that was not properly imaged or there may be a change in rock property that prevents proper imaging. In any case, the anticline is likely underlain by the Bardibas thrust and given the proximity of the Ratu River line, we interpret that this structure represents an earlier stage of the Bardibas fault and fold imaged beneath the Ratu River, which contains elements of both pure-shear fault-bend folding and fault-propagation folding.

Although we cannot quantitatively describe the kinematics of folding in this profile, we note that the shallow stratigraphy is well imaged and shows a spectacular unconformity above tilted Siwalik strata (yellow arrows in Fig. 6). Above the unconformity, we observe continuous, nearly horizontal, well bedded strata, which are in turn overlain by a layer without clear bedding that extends to the surface. We interpret these post-Siwalik strata as Quaternary fluvial sediments.

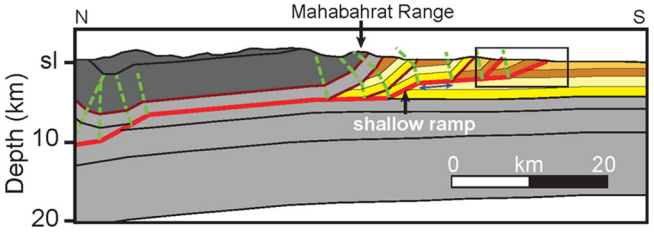

Fig. 7. Southern section of the general cross-section of Fig. 1A redrawn to show the shallow ramp inferred to exist north of the Ratu seismic profile. Bold red line indicates active faults, thin dark red lines represent inactive faults and green dashed lines represent axial surfaces. The double headed blue arrow represents the offset of the first inactive fault from the shallow ramp, equivalent to the accumulated slip on the two active fault strands. Black box shows area of Ratu seismic profile.

5. Discussion

5.1. New findings

5.1.1. The décollement is shallow and steps down on a ramp below the sub-Himalaya

Typically, the décollement at the base of the MFT is considered to be 5 km below the surface (e.g., Lave and Avouac, 2000; Hirschmiller et al., 2014). In contrast, our imaging (Fig. 2) shows that the MFT near Bardibas flattens at ~2 km below the surface. The lack of deformation to the south of our seismic section indicates that there is no deeper décollement, below our imaging that could transfer slip into the foreland.

Our interpretation implies that the depth of the décollement changes both along strike and down-dip. Approximately 2 km north of our profile termination, the Kamala thrust (Fig. 1) exposes Lower Siwalik units, whereas the Bardibas and Patu thrusts sole into Middle Siwalik rocks. Thus the Kamala thrust must sole into a deeper stratigraphic level and there must be a step in the MHT linking the décollement observed in our seismic profile with this deeper décollement (Fig. 7). The base of the Kamala thrust will be offset from this ramp by the amount of shortening accrued by the Patu and Bardibas thrusts. Along strike, we can also infer changes in the depth of the décollement. For example, Lave and Avouac (2000) use structural and stratigraphic measurements to propose that the décollement is at 5 km below the surface at a location

45 km to the west of our profile and Lee et al. (2017) use a combination of seismic profiles and surface measurements to infer the same for the décollement underlying the Triyuga piggy-back basin.

The shallow décollement level that we identify, however, may be characteristic of other locations along the Himalayan range front. Published cross-sections across the MFT in the Himalaya of northwest India, ∼860 and 1100 km to the west of our seismic line (Powers et al., 1998), show that Middle Siwalik strata dip 30° to the north, slightly steeper than the interpreted dip of the MFT at the surface (35°, though this is unconstrained by subsurface data). This is consistent with the MFT there flattening at the same stratigraphic interval as the MFT beneath the Ratu River, suggesting that this shallow décollement exists at multiple locations along the range front.

5.1.2. The Bardibas thrust is blind at the Ratu River

We observe that the Bardibas thrust does not reach the surface (Figs. 2, 3). Although the MFT is typically drawn at the topographic break between the Siwalik Group and the younger fluvial sediments, this is not the case at the Ratu River. Rather, the kink-band observed in the shallow sub-surface suggests that the uppermost deformation is accommodated by folding. In contrast, the Patu thrust is clearly imaged as surface emergent (Fig. 2).

Further, the geometry of the shallow kink band raises the possibility that the shallowest layers may capture the deformation related to the past two great earthquakes in this region, with ∼15 m of uplift accommodated during those two events. The abrupt change in the width of the kink band suggests that, at this scale, the kink band has developed in a step wise manner. The fact that the youngest section of the kink band is more or less half the width of the deeper section of the kink band also suggests that the latter has formed during two earthquakes and the former corresponds to only one. The amount of total uplift across the kink band (15 m) would be consistent with two great earthquakes similar to those observed in trenches in the region (e.g. Lave et al., 2005; Sapkota et al., 2013). In addition, we note that the sediments affected by this kink band onlap onto a deeper fold in the fluvial sediments (red arrows in Fig. 3B), indicating that prior to this phase of deformation, the tip of the fault was causing folding ∼400 m north of the present location, with at least 50 m of total uplift.

It should be expected that some strands of the MFT are blind. Across the sub-Himalaya, we find many locations with asymmetrical frontal folds like the one in Bardibas (e.g., Chandigarh anticline, Malik and Nakata, 2003; Ramnagar anticline, Kumar et al., 2006), a feature that is typical of faults that have propagated towards the surface over time (Jamison, 1987; Hughes and Shaw, 2015). In particular, blind faults are expected close to lateral fault terminations; our profile is located near the western tip of the Bardibas thrust, where slip should be tapering to zero (Dawers and Anders, 1995). Indeed, slip does increase to the east: the Bardibas thrust breaches the surface at the Charnath River (Fig. 1; Sapkota, 2011).

5.1.3. Direct measurements of fault and bedding dip

We can directly measure apparent bedding and fault attitudes from our seismic profiles. The Bardibas thrust dips slightly more gently (∼20–30°) than the Patu thrust (28°–39°). This difference in dip also reflects a change in folding mechanism. In the Patu thrust, the axial surface that defines the northern extent of the backlimb bisects the fold, indicating that the beds are deforming by flexural slip and that this is a fault-bend fold. Surprisingly, the Bardibas thrust exhibits a different structural style within the same stratigraphic section. The Bardibas thrust backlimb is wide and dips more gently (∼10–14°) than the fault (∼20°), which is characteristic of a fault with rocks deforming by shear in the basal layers of the hanging-wall (Fig. 2). Although we initially considered that this difference in structural style was due to the Patu thrust being a more mature fault (i.e. it had accrued more slip), in fact the amounts of shortening are not significantly different (1.8 km for the Patu thrust vs 1.7 km for the Bardibas thrust).

5.1.4. Sediment supply and base level changes affect river incision

In the footwall of the Bardibas thrust, the depth of the base of the low-velocity fluvial sediments south of the topographic front in the Ratu River indicates that in the past, the local base level there was 100–200 m lower than it is today (Fig. 3). Further, the incised valley observed in the Ratu river profile suggests that such base level changes have occurred several times in the past: of the ∼90 m of incision, at least the upper half is into fluvial sediments (as identified by the fine layering of seismic reflections and slow seismic velocities) that must have been deposited in a previous phase of aggradation. The fact that these changes occur in the footwall of the Bardibas thrust suggests that they reflect fluvial dynamics rather than slip on the thrust. Consequently, in our seismic line we preserve evidence of at least one phase of post-Upper Siwalik aggradation, later valley incision, and a subsequent phase of aggradation. We do not have ages of the strata, so we cannot determine the timing of the evolution, however, we can determine the relative timing of the stages of deposition and erosion. Fig. 4 shows a schematic of the different stages of stratigraphic evolution of this area as well as the relative rise and fall of base level implied by the preserved strata.

The angular unconformity imaged under the Bhabsi River (Fig. 6), in the hanging wall of the Bardibas thrust, indicates that the local base level there was at least 80 m lower than the present river level (this is a minimum, as the unconformity has probably been uplifted along with the rest of the hanging wall). In tectonically active regions, tectonic uplift is generally considered to be the main driver of local base level change and river incision (Bull, 2007), but this assumption would lead to the flawed conclusion that the hanging wall of the Bardibas thrust subsided and created the accommodation space for the Quaternary fluvial sediments overlaying the angular unconformity. This angular unconformity is analogous to the strath surfaces uplifted above the Ratu River, both of which are in the hanging wall of the Bardibas thrust.

We suggest that non-tectonic factors such as sediment supply, regional subsidence rate, and climactic variations must also play an important role in forming strath surfaces around the MFT, as has been proposed elsewhere in the Himalaya (Dingle et al., 2016) and other regions (e.g., Fuller et al., 2009; Bufe et al., 2016). Millennial-scale variations in monsoon intensity play a fundamental role in modulating sediment supply to the foreland of the Himalaya (Bookhagen et al., 2005). This can result in sediment pulses, as observed in the High Himalaya of Central Nepal at ∼7 ka (Pratt et al., 2002) and in fill terrace formation episodes in intermontane valleys of the Sub-Himalaya (e.g., Singh and Tandon, 2010; Dutta et al., 2012), as well as changes in the depositional slope of the piedmont alluvial fans, which can change local base-level upstream (Blair and McPherson, 2009). Given that the oldest dated terraces above the current river level in the hanging wall of the Bardibas thrust (T5 of Bollinger et al., 2014, dated to ∼7 ka) are 60–70 m above present-day river level (on the same order as the base level variations observed in our seismic profiles), these other effects are likely to have a significant impact on interpreted uplift rates. These scenarios suggest that the steady-state topography assumption (i.e. that erosion balances rock uplift) built into many geomorphic and structural models (e.g., Kirby and Whipple, 2001; Miller et al., 2007) are likely insufficient for this region.

5.2. Implications of our results for seismic hazard studies in Nepal

If earthquake scientists continue to rely solely on trenching and terraces to assess shortening and earthquake history, we are likely to underestimate seismic hazard. Future efforts to fully constrain seismic hazards in the Himalaya must take a more comprehensive approach. A combination of geophysical imaging and shallow drilling to characterize long-term shortening rates has been used in central Japan (Ishiyama et al., 2007) and southern California (Hubbard et al., 2014; McAuliffe et al., 2015). Our successful imaging of the MFT suggests that this strategy can also be applied in central Nepal.

Our study has implications for the earthquake segmentation processes in the region. Many studies have argued for a deep ramp beneath the High Himalaya that represents the downdip limit of seismic locking (e.g. Stevens and Avouac, 2015). Hubbard et al. (2016) argue for a second ramp that caused the updip termination of slip in the 2015 Gorkha earthquake. Here, our interpretation of a third, shallower ramp that separates the décollement at the base of the Lower Siwalik from the décollement in the Middle Siwalik, suggests that there may be additional geometric barriers to earthquake rupture. Slip on this ramp would uplift the rocks above it, and may be responsible for the steep topography of the Mahabharat range south of Kathmandu (Fig. 7). Given that the depth below the surface of the frontal décollement of the MFT has been documented at both 5 km (Lave and Avouac, 2000) and 2 km (this study), the ramp must have a complex shape along strike.

This study also highlights the importance of carrying out a detailed site assessment for paleoseismological studies. Trenching along the topographic break will not find surface ruptures of the MFT in locations where the fault is blind, so in these cases, we must rely on terrace uplift rates to assess fault slip. However, kinematic modeling of blind versus emergent faults shows that understanding the fault system is critical. Uplift rates above propagating faults can be twice as high as above emergent faults for the same shortening rate (Hubbard et al., 2014). If blind faults are assumed to be emergent, this could lead to significantly incorrect estimates of shortening and slip rate. In any case, terrace uplift data provide average kinematic rates rather than an earthquake history.

From a hazards perspective, it is critical to have an accurate location of the fault trace. Studies of fatalities related to the Chi-Chi earthquake that occurred in Taiwan in 1999 showed that the great majority of fatalities occurred within 100 m of the surface trace of the fault, and the fatality rate was higher on the hanging wall than on the footwall of the seismogenic fault (Pai et al., 2007). Our study shows how the tip of the blind MFT is located $\sim$1 km south of the range front, thus shifting the fatality zone into the densely populated plains just south of the topographic break. This illustrates how having the accurate location of the fault can allow for more effective hazard management planning.

Our study has shown that high resolution seismic data may be able to image not only the geometry of the strata and faults in the subsurface, but also the kinematic evolution of the fault at the detail of individual earthquakes. It may also be possible to assess earthquake histories by identifying and dating colluvial wedges (e.g., the Thapatol trench along the Bardibas thrust; Bollinger et al., 2014) and then linking them to earthquakes (Jibson, 2009). This would be a terrestrial analog to inferring the earthquake history of the Cascadia margin using the ages of turbidite deposits (Goldfinger et al., 2012). However, this would require very thorough trenching and dating studies over wide areas of the range front.

Neotectonic studies in the Himalaya that use uplift measurements of geomorphic surfaces require a fault dip to infer fault slip. Through seismic imaging, we show that the dip of the fault can vary significantly, even along the same fault. If not properly accounted for, this could lead to incorrect slip estimates, as well as incorrectly correlated terrace treads. For faults with a well-defined backlimb axial surface and a backlimb dipping 25°–35°, like the Patu thrust, measured bed dips are likely a more accurate constraint on fault dip than measurements of the fault itself in the upper few meters. In contrast, for faults with a wide and gently dipping backlimb, such as the Bardibas thrust, the fault likely dips more steeply than the hanging wall beds, although it may still have a gentle dip.

Using strath terrace uplift rates to infer tectonic uplift rates requires constraints on base level changes through time. Here, we show that the base level in the frontal Himalaya has gone up and down since the deposition of the Upper Siwalik strata. Although this effect has been well studied at different locations along the Himalayan range front for fill terraces and terraces incising older Quaternary features such as alluvial fans, (e.g. Suresh et al., 2007; Singh and Tandon, 2010; Dutta et al., 2012), few studies have thoroughly considered the effect of base level changes on the development of strath terraces (e.g. Lave and Avouac, 2000). However, these studies have found a strong relationship between the monsoon intensity and terrace development. Further quantifying this effect will require detailed studies of Quaternary fluvial sediments to determine their age and deposition rates, as well as the age of both the erosional surfaces that are buried (e.g. Fig. 6) and their uplifted equivalents. Lacking such information, however, uplift estimates measured from strath terraces must incorporate larger uncertainties to account for this effect.

6. Conclusions

We present two pre-stack depth migrated seismic profiles from the Bardibas region of Nepal that clearly image the deformation associated with displacement along the youngest frontal ramps of the MFT system, locally called the Bardibas and Patu Thrusts. These seismic lines allow us to determine that the strata form fault-bend folds of different styles above the thrusts. From the geometry of the fold above the Patu thrust, we can robustly infer the depth to the decollement beneath these structures and show that is $\sim$2 km, shallower than the depth observed at other locations. We also show that the southernmost fault ramp, the Bardibas thrust, is blind and deformation reaches the surface as folding of fluvial sediments. We are also able to directly measure the dips of the faults at depth. There is evidence of changes of base level on the order of 80–90 m, preserved in both the hanging wall and foot wall of the Bardibas thrust. These include regional beveling of the Bardibas anticline below the Bhabsi River and the formation of incised valleys following fluvial aggradation south of the Bardibas thrust. This suggests that fluvial dynamics may be an important factor in the formation of strath terraces in this region.

Earthquakes along the Himalaya represent one of the greatest seismic hazards in the world. Understanding how and where great earthquakes have ruptured in the past is critical to assessing future hazard. We present the first active-source seismic reflection images of the MFT at depth, and demonstrate that the paleoseismic record is complicated by blind fault strands and changes in sedimentation patterns. This highlights the importance of carefully evaluating the structural context of trench and terrace studies. A failure to do so could result in an incomplete earthquake history.

Acknowledgements

This research is supported by the National Research Foundation Singapore (NRF) and the Singapore Ministry of Education under the Research Centres of Excellence initiative and the NRF Fellowship scheme (award No. NRF-NRFF2013-06). This work comprises Earth Observatory of Singapore contribution no. 194. The authors

thank Chintan Timsina, Roshan Koirala, Pramod Simkhada, Ratnamani Gupta, Peter Polivka, Dana Peterson, and Paula Bürgi for their assistance in the field; Yixiang Liu for her assistance with processing; and Kyle Bradley, Paul Tapponnier and Cagil Karakas for useful discussions. We thank Landmark for providing the SeisSpace software package used to process the seismic data.

Appendix A. Supplementary material

Supplementary material related to this article can be found online at https://doi.org/10.1016/j.epsl.2018.04.045. These include a Google map file with the locations of the CDP's used for the processing of the seismic profiles described in this article.

References

Bilham, R., 2014. Aggravated earthquake risk in South Asia: engineering versus human nature. In: Wyss, M., Shroder, J.F. (Eds.), Earthquake Hazard, Risk, and Disasters. In: Hazards and Disasters Series. Elsevier Publishing, pp. 103–141.

Blair, T.C., McPherson, J.G., 2009. Alluvial fan processes and forms. In: Abrahams, A.D., Parsons, A.J. (Eds.), Geomorphology of Desert Environments, 2nd ed. Springer Link Publishing, pp. 413–467.

Bollinger, L., et al., 2014. Estimating the return times of great Himalayan earthquakes in eastern Nepal: evidence from the Patu and Bardibas strands of the Main Frontal Thrust. J. Geophys. Res., Solid Earth 119. https://doi.org/10.1002/2014JB010970.

Bookhagen, B., Thiede, R.C., Strecker, M.R., 2005. Late Quaternary intensified monsoon phases control landscape evolution in the northwest Himalaya. Geology 33, 149–152.

Bufe, A., Paola, C., Burbank, D.W., 2016. Fluvial bevelling of topography controlled by lateral channel mobility and uplift rate. Nat. Geosci.. https://doi.org/10.1038/NGEO2773.

Bull, W.B., 2007. Tectonic Geomorphology of Mountains. Blackwell Publishing. 316 pp.

Dalrymple, R.W., Boyd, R., Zaitlin, B.A., 1994. History of research, types and internal organisation of incised-valley systems: introduction to the volume. In: Dalrymple, R.W., Boyd, R., Zaitlin, B.A. (Eds.), Incised Valley Systems: Origins and Sedimentary Sequences, Society of Economic Petrologists and Mineralogists Special Publication 51, p. iii.

Dawers, N.H., Anders, M.H., 1995. Displacement-length scaling and fault linkage. J. Struct. Geol. 17, 607–614.

DeCelles, P.G., Giles, K.A., 1996. Foreland basin systems. Basin Res. 8, 105–123.

Delcaillau, B., 1992. Les Siwaliks de l'Himalaya de Nepal Oriental: fonctionnement et evolution d'un piedmont. Editions du Centre National de la Recherche Scientifique. 205 pp.

Dhital, M.R., 2015. Geology of the Nepal Himalaya: Regional Perspective of the Classic Collided Orogen. Springer International Publishing, Switzerland. 498 pp.

Dingle, E., Sinclair, H., Attal, M., Milodowski, D., Singh, V., 2016. Subsidence control on river morphology and grain size in the Ganga Plain. Am. J. Sci. 316, 778–812.

Dubille, M., Lave, J., 2015. Rapid grain size coarsening at sandstone/conglomerate transition: similar expression in Himalayan modern rivers and Pliocene molasse deposits. Basin Res. 27, 26–42.

Dutta, S., Suresh, N., Kumr, R., 2012. Climatically controlled Late Quaternary terrace staircase development in the fold-and-thrust belt of the Sub Himalaya. Palaeogeogr. Palaeoclimatol. Palaeoecol. 356–357, 16–26.

Fuller, T.K., Perg, L.A., Willenbring, J.K., Lepper, K., 2009. Field evidence for climate-driven changes in sediment supply leading to strath terrace formation. Geology 37, 467–470.

Gansser, A., 1964. Geology of the Himalayas. Interscience, London. 289 p.

Goldfinger, C., et al., 2012. Turbidite Event History – Methods and Implications for Holocene Paleoseismicity of the Cascadia Subduction Zone. U.S. Geological Survey Professional Paper 1661-F, 170 p.

Hirschmiller, J., Grujic, D., Bookhagen, B., Coutand, I., Huyghe, P., Mugnier, J-L., Ojha, T., 2014. What controls the growth of the Himalayan foreland fold-and-thrust belt? Geology 42, 247–250.

Hubbard, J., Almeida, R., Foster, A., Sapkota, S., Bürgi, P., Tapponnier, P., 2016. Structural segmentation controlled the 2015 Mw 7.8 Gorkha earthquake rupture in Nepal. Geology 44, 639–642.

Hubbard, J., Shaw, J.H., Dolan, J., Pratt, T.L., McAuliffe, L., Rockwell, T.K., 2014. Structure and seismic hazard of the Ventura Avenue anticline and Ventura fault, California: prospect for large, multi-segment ruptures in the western Transverse Ranges. Bull. Seismol. Soc. Am. 104, 1070–1087. https://doi.org/10.1785/0120130125.

Hughes, A.N., Shaw, J.H., 2015. Insights into the mechanics of fault-propagation folding styles. Geol. Soc. Am. Bull. 127, 1752–1765.

Ishiyama, T., Mueller, K., Sato, H., Togo, M., 2007. Coseismic fault-related fold model, growth structure, and the historic multi-segment blind thrust earthquake on the basement-involved Yoro thrust, central Japan. J. Geophys. Res. 112, B03S07. https://doi.org/10.1029/2006JB004377.

Jamison, W.R., 1987. Geometric analysis of fold development in overthrust terranes. J. Struct. Geol. 9, 207–219.

Jarvis, A., Reuter, H.I., Nelson, A., Guevara, E., 2008. Hole-filled SRTM for the globe Version 4. Available from the CGIAR-CSI SRTM 90m Database: http://srtm.csi.cgiar.org.

Jibson, R.W., 2009. Using landslides for paleoseismic analysis. In: McCalpin, J.P. (Ed.), Paleoseismology, 2nd edition. In: International Geophysics Series, vol. 95. Elsevier Publishing, pp. 565–601.

Kirby, E., Whipple, K.X., 2001. Quantifying differential rock-uplift rates via stream profile analysis. Geology 29, 415–418.

Kumar, S., et al., 2006. Paleoseismic evidence of great surface-rupture earthquakes along the Indian Himalaya. J. Geophys. Res. 111, B03304. https://doi.org/10.1029/2004JB003309.

Lave, J., Avouac, J.-P., 2000. Active folding of fluvial terraces across the Siwaliks Hills, Himalayas of central Nepal. J. Geophys. Res. 105, 5735–5770.

Lave, J., et al., 2005. Evidence for a great Medieval earthquake (~1100 A.D.) in the central Himalayas, Nepal. Science 307, 1302–1305.

Lee, Y.S., et al., 2017. Development of piggy-back basins in the Sub-Himalaya, structure of the Triyuga Valley in Eastern Nepal from seismic reflection profiles. In: American Geophysical Union Fall Meeting.

Malik, J.N., Nakata, T., 2003. Active faults and related Late Quaternary deformation along the northwestern Himalayan Frontal Zone, India. Ann. Geophys. 46, 917–936.

McAuliffe, L.J., Dolan, J.F., Rhodes, E.J., Hubbard, J., Shaw, J.H., Pratt, T.L., 2015. Paleoseismologic evidence for large-magnitude (Mw 7.5–8.0) earthquakes on the Ventura blind thrust fault: implications for multi-fault ruptures in the Transverse Ranges of southern California. Geosphere 11, 1629–1650.

Miller, S.R., Slingerland, R.L., Kirby, E., 2007. Characteristics of steady-state fluvial topography above fault-bend folds. J. Geophys. Res., Earth Surf. 112, F04004. https://doi.org/10.1029/2007JF000772.

Mitra, S., 2002. Structural models of faulted detachment folds. Am. Assoc. Pet. Geol. Bull. 86, 1673–1694.

Nakata, T., et al., 1998. First successful paleoseismic trench study on active faults in the Himalaya. Eos, Trans. Am. Geophys. Union 79, 615.

Pai, C.-H., Tien, Y.-M., Teng, T.-L., 2007. A study of the human-fatality rate in near-fault regions using the Victim Attribute Database. Nat. Hazards 42, 19–35.

Powers, P.M., Lillie, R.J., Yeats, R.S., 1998. Structure and shortening of the Kangra and Dehra Dun reentrants, Sub-Himalaya, India. Geol. Soc. Am. Bull. 110, 1010–1027.

Pratt, B., Burbank, D.W., Heimsath, A., Ojha, T., 2002. Impulsive alluviation during early Holocene strengthened monsoons, central Nepal Himalaya. Geology 30, 911–914.

Sapkota, S.N., 2011. Surface Rupture of the 1934 Bihar–Nepal Earthquake: Implications for Seismic Hazard in Nepal Himalaya. Ph.D Thesis. Institute Physics du Globe, Paris. 291 p.

Sapkota, S.N., Bollinger, L., Klinger, Y., Tapponnier, P., Gaudemer, Y., Tiwari, D., 2013. Primary surface rupture of the great Himalayan earthquakes of 1934 and 1255. Nat. Geosci. 6, 71–76.

Schelling, D., Arita, K., 1991. Thrust tectonics, crustal shortening and the structure of the far-eastern Nepal Himalaya. Tectonics 10, 851–862.

Seeber, L., Armbruster, J., 1981. Great detachment earthquakes along the Himalayan Arc and long-term forecasting. In: Simpson, D.W., Richards, P.G. (Eds.), Earthquake Prediction: An International Review. In: Maurice Ewing Series, vol. 4. American Geophysical Union, pp. 259–277.

Shaw, J.H., Connors, C., Suppe, J., 2005. Interpretation of Contractional Fault-Related Folds: An AAPG Seismic Atlas. AAPG Special Publication 48.

Singh, V., Tandon, S.K., 2010. Integrated analysis of structures and landforms of an intermontane longitudinal valley (Pinjaur dun) and its associated mountain fronts in the NW Himalaya. Geomorphology 114, 573–589.

Stevens, V., Avouac, J.-P., 2015. Coupling on the Main Himalayan Thrust. Geophys. Res. Lett. 42, 5828–5837.

Suppe, J., 1983. Geometry and kinematics of fault-bend folding. Am. J. Sci. 283, 684–721.

Suppe, J., Connors, C.D., Zhang, Y., 2004. Shear fault-bend folding. AAPG Mem. 82, 303–323.

Suresh, N., Bagati, T.N., Kumar, R., Thakur, V.C., 2007. Evolution of Quaternary alluvial fans and terraces in the intramontane Pinjaur Dun, Sub-Himalaya, NW India: interaction between tectonics and climate change. Sedimentology 54, 809–833.

Wesnousky, S.G., et al., 1999. Uplift and convergence along the Himalayan Frontal Thrust of India. Tectonics 18, 967–976.

Wesnousky, S.G., et al., 2017. Geological observations on large earthquakes along the Himalayan frontal fault near Kathmandu, Nepal. Earth Planet. Sci. Lett. 457, 366–375.

Zhao, W., Nelson, K.D., INDEPTH Team, 1993. Deep seismic reflection evidence for continental underthrusting beneath southern Tibet. Nature 366, 557–559.